Neurotropic Virus Tracing Suggests a Membranous-Coating-Mediated Mechanism for Transsynaptic Communication

Yan-Chao Li,[1,2]* Wan-Zhu Bai,[2,3] Norio Hirano,[4]* Tsuyako Hayashida,[2] Takahide Taniguchi,[5] Yoichi Sugita,[6,7] Koujiro Tohyama,[2,8] and Tsutomu Hashikawa[2,7]*

[1]Department of Histology and Embryology, Norman Bethune College of Medicine, Jilin University, Changchun, Jilin Province 130021, China
[2]Neural Architecture, Advanced Technology Development Group, RIKEN Brain Science Institute, Saitama 351-0198, Japan
[3]Institute of Acupuncture and Moxibustion, China Academy of Chinese Medical Science, Beijing 100700, China
[4]Department of Veterinary Microbiology, Iwate University, Morioka, Iwate 020-8550, Japan
[5]Division of Animal Science, Institute of Symbiotic Science and Technology, Tokyo University of Agriculture and Technology, Fuchu, Tokyo 183-8509, Japan
[6]Cognitive and Behavioral Science Group, AIST Neuroscience Research Institute, Tsukuba, Ibaraki 305-8568, Japan
[7]Core Research for Evolutional Science and Technology (CREST), Japan Science and Technology Agency, Chiyoda, Tokyo 102-0075, Japan
[8]Center for EM and Bio-Imaging Research, Iwate Medical University, Morioka, Iwate 020-8505, Japan

ABSTRACT

Swine hemagglutinating encephalomyelitis virus (HEV) has been shown to have a capability to propagate via neural circuits to the central nervous system after peripheral inoculation, resulting in acute deadly encephalomyelitis in natural host piglets as well as in experimental younger rodents. This study has systematically examined the assembly and dissemination of HEV 67N in the primary motor cortex of infected rats and provides additional evidence indicating that membranous-coating-mediated endo-/exocytosis can be used by HEV for its transsynaptic transfer. In addition, our results suggested that this transsynaptic pathway could adapted for larger granular materials, such as viruses. These findings should help in understanding the mechanisms underlying coronavirus infections as well as the intercellular exchanges occurring at the synaptic junctions. J. Comp. Neurol. 521:203–212, 2013.

© 2012 Wiley Periodicals, Inc.

INDEXING TERMS: coronavirus; virus replication; transsynaptic transfer; neurons

Swine hemagglutinating encephalomyelitis virus (HEV) is a positive, nonsegmented, single-stranded RNA coronavirus belonging to the betacoronaviruses, together with mouse hepatitis virus, bovine coronavirus, human coronavirus OC43, and severe acute respiratory syndrome coronavirus (Masters, 2006; De Groot et al., 2012). As the first member of the group of coronaviruses found to invade the central nervous system (CNS), HEV was initially isolated from encephalomyelitic piglet brains in 1960 in Canada by Greig et al. (1962). Subsequent studies demonstrated that HEV first oronasally infects the epithelial cells lining the respiratory tract and small intestine and thereafter is delivered retrogradely via peripheral nerves to the central neurons in charge of peristaltic function of the digestive tract, resulting in the so-called vomiting diseases (Andries and Pensaert, 1980).

© 2012 Wiley Periodicals, Inc.

Early electron microscopic (EM) and virological analysis showed that glial cells were not infected by HEV in primarily cultivated astrocytes (Yagami et al., 1993) or in the brains of infected piglets or mice (Meyvisch and Hoorens, 1978; Yagami et al., 1986), indicating that

Grant sponsor: RIKEN Brain Science Institute; Grant number: G29 (to T.Has.); Grant sponsor: MEXT Japan; Grant number: 15650066 (to K.T., T.Has.).

*CORRESPONDENCE TO: Yan-Chao Li, Department of Histology and Embryology, Norman Bethune College of Medicine, Jilin University, Changchun, Jilin Province 130021, China. E-mail: ldlyc@yahoo.com; or Norio Hirano, Department of Veterinary Microbiology, Iwate University, Morioka, Iwate 020-8550, Japan. E-mail: nhirano@iwate-u.ac.jp or Tsutomu Hashikawa, Neural Architecture, Advanced Technology Development Group, RIKEN Brain Science Institute, Saitama 351-0198, Japan. E-mail: tom@brain.riken.jp

Received January 18, 2012; Revised February 14, 2012; Accepted June 7, 2012
DOI 10.1002/cne.23171
Published online June 14, 2012 in Wiley Online Library (wileyonlinelibrary.com)

neurons are the major target of HEV in the CNS. However, previous in vivo studies concentrated mainly on the later stage of infection, and it is not clearly understood how this virus is replicated within and released from the central neurons.

Recently we examined HEV-infected rat dorsal root ganglia (DRG) and found that HEV in the cell bodies of infected sensory neurons budded from endoplasmic reticulum–Golgi intermediate compartments and was assembled either individually within small vesicles or in groups within large vesicles. The progeny virions were released from the sensory neurons mainly by the large, smooth-surfaced, vesicle-mediated secretory pathway (Li et al., 2012).

In the present study, systematic electron microscopy (EM) and morphological analysis were employed to obtain detailed insights into the replication and dissemination of HEV in the CNS. A plaque-cloned HEV 67N strain (Hirano et al., 1990) was used, which has previously been demonstrated to be confined exclusively to neurons (Hirano et al., 1994; Bai et al, 2006; Li et al., 2012). Preliminary EM analysis of HEV-infected motor cortices showed that the pyramidal cells remained largely intact at day 4 post-infection (p.i.) and that both the cytoplasmic and the perineuronal architectures maintained their normal morphology. Destructive changes in the infected neurons did not become prominent until day 5 p.i., which was coincident with the recruitment of immune cells to the infected areas. Therefore, the brains collected at day 4 p.i. were used in this experiment to obtain detailed insights into the replication and dissemination of HEV in the CNS.

MATERIALS AND METHODS

Virus and animals

HEV 67N strain, also called the *North American strain*, was initially isolated from the nasal cavity of apparently healthy swine in Iowa, during a routine survey for viruses harbored in the respiratory tract by Mengeling et al. (1972). This virus was obtained from Dr. W.L. Mengeling (National Animal Disease Laboratory, Ames, IA). Specific-pathogen-free male Wistar rats (4 weeks old, ~70–90 g), serologically negative for MHV infections, were purchased from SLC (Hamamatsu, Japan).

Cell culture and plaque assay

HEV 67N was passaged 12 times in primary porcine kidney cell cultures (Hirai et al., 1974) and more than 10 times in suckling mouse brains by intracerebral inoculation. The mouse-brain-adapted HEV 67N strain was plaque-purified three times in an established swine kidney cell line and thereafter was propagated 20 times in the same cell line until use. The viral supernatant from infected cell culture, with a titer of 10^6 PFU/0.2 ml as assayed by plaque method, was kept at −80°C and was used for all experiments. Swine kidney cell culture and plaque assay of the virus were carried out as described by Hirano et al. (1990).

Anti-HEV antibody preparation

Four-week-old mice were inoculated intraperitoneally twice with 0.2 ml HEV 67N strain at an interval of 2 weeks; at 1 week after the last inoculation, mice were killed to collect the blood. The antiserum was heated at 56°C for 30 minutes, and the specificity was examined by neutralization and hemagglutinating inhibition tests (Yagami et al., 1986; Hirano et al, 1990).

Animal inoculation

Thirteen rats were inoculated by injecting 200 μl viral culture supernatant (10^6 PFU) into the right hind foot pad with a 1-ml syringe. Three rats were inoculated with virus-free cell culture supernatant as vehicle controls. All the rats were reared separately in cages, with food and water freely available. All the experiments with active virus were carried out in Biosafety Level 2 containment and performed in accordance with the NIH *Guide for the care and use of laboratory animals*.

HEV antigen detection in the CNS

Three HEV-infected rats were perfused at day 4 p.i. through the heart with 50 ml physiological saline under halothane anesthesia (Fluothane; Takeda Pharmaceutical, Osaka, Japan), followed by 200–300 ml 4% paraformaldehyde in 0.1 M phosphate buffer (PB; pH 7.4). The brains were dissected out, postfixed in fresh fixatives for 4–6 hours, and then washed in a series of cold sucrose solutions of increasing concentration. The samples were embedded in OCT compound (Tissue-Tek; Sakura Finetek Japan, Tokyo, Japan), frozen on dry ice, then cut into 40-μm-thick transverse sections with a freezing microtome.

The cryosections were preincubated with 3% normal goat serum in 0.1 M PB containing 0.1% Triton X-100 for 30 minutes at room temperature, then incubated with the mouse anti-HEV antibody overnight at 4°C. After several washes with 0.1 M PB, the sections were reacted with Alexa 594-conjugated goat anti-mouse IgG antibody (Molecular Probes, Eugene, OR) in 0.1 M PB for 60 minutes at room temperature. The specificity of the primary antibody has been reported previously (Hirano et al., 1990) and was verified in this study by replacing the antiviral antibody with 0.1 M PB. The sections were mounted onto glass slides with Immu-Mount (Shandon, Pittsburgh, PA) and examined with a laser scanning confocal microscope (FV1000; Olympus, Tokyo, Japan).

Systematical ultrastructural investigations of HEV in the CNS

Ten infected rats and three vehicle-injected rats were perfused at day 4 p.i. through the heart with 50 ml physiological saline under halothane anesthesia, followed by 200–300 ml of fixatives containing 2% glutaraldehyde and 2% tanic acid in 0.1 M PB. The brains were dissected out, postfixed in fresh fixatives for 4–6 hours, and then left in 0.1 M PB containing 5% sucrose overnight at 4°C. Serial coronal sections of rat brains about 50 μm thick were cut on a DSK microslicer (DTK-1000, Zero-1; Dosaka EM, Kyoto, Japan).

The sections were fixed in 1% osmium tetroxide in 0.1 M PB for 2 hours at 4°C, dehydrated in increasing concentrations of ethanol, and embedded in Epon 812. Ultrathin sections about 80 nm thick were cut on an Ultracut E ultramicrotome (Reichert-Jung, Wien, Austria) and collected on Formvar-coated grids. The ultrathin sections were stained with uranyl acetate and lead citrate and then examined with a transmission electron microscope (Technai 12 FEI).

Morphological analysis

High-resolution EM images were recorded on Image Plates (FujiFilm, Tokyo, Japan), which were scanned with Fujifilm FDL 5000 and converted into digital images with the software Image Gauge 4.0 (FujiFilm). The brightness and contrast of each image file were uniformly adjusted with this software. The dimensions of cells and virions were measured on electron micrographs with Olympus Soft Imaging 1.2 (Olympus Soft Imaging Solutions GmbH, Münster, Germany). Final pictures were prepared in Adobe Photoshop 6.0 (Adobe Systems, San Jose, CA).

RESULTS

Localization of HEV-positive cells in the CNS

The involved neural circuits and the temporal patterns of infected neuron groups after inoculation have been characterized previously (Hirano et al., 1994; Bai et al., 2006; unpublished data). These experiments showed that footpad inoculation of HEV in 4-week-old rats consistently resulted in the ipsilateral infection of DRG (∼L4–L6) and spinal motoneurons at lumbar levels at day 3 p.i. and in the contralateral infection of layer V of the hind limb area in the primary motor cortex at day 4 p.i. Infected rats showed a relatively constant onset of encephalomyelitis, with an average survival of about 6 days. Fatal infection with HEV can be protected against by cutting the proximal segment of the sciatic nerve within 1 hour after inoculation (Hirano et al., 1995). Moreover, no anterograde propagation of HEV has been found along spinal ascending pathways throughout the periods examined (Bai et al., 2006; unpublished data). Consistent with the results in the previous experiments, the present study showed that at day 4 p.i. HEV-positive cells were observed in only a certain population of neurons with different sizes in layer V of the primary motor cortex (Fig. 1A,B). The fluorescence signals for HEV showed a punctate pattern and were located in the cell bodies and the primary dendrites of pyramidal cells (Fig. 1C). By contrast, less intense staining was also seen in the putative axons (arrows in Fig. 1C).

Ultrastructural characteristics of HEV

Usually, it is not easy to examine virus particles ultrastructurally in vivo, even if the viral antigen has been labeled by immunostaining, because virions are very small, and viral structures or vesicular membrane cannot be identified clearly because of the immunostaining reaction. Therefore, the ultrastructural analysis was focused mainly on the layer V pyramidal neurons in the hind limb representation of motor cortex, and only unstained sections were used.

Ultrastructural examinations showed that virus particles were distributed in axons (Fig. 1F–H), perikarya (Figs. 1E, 2C,D), and dendrites (Fig. 2A,B,E) but not in the nucleus (Fig. 1E) and were undetectable in control materials (Figs. 2G, 3E–H). Under EM, intracellular virus was identified as spherical particles inside vesicles or as electron-dense materials in the process of budding into the intracellular membranous cisternae, as reported previously (Clarke and McFerran, 1971; Mengeling et al., 1972; Yagami et al., 1986). Enveloped virus particles were spherical, with an electron-lucent or -dense center, and the outer surfaces of the viral envelopes were often covered by a layer of well-defined projections, forming a typical “corona” profile (Fig. 2F1,2). The number of virus particles per cell varied greatly from cell to cell, suggesting that the severity of infection was different among neurons even at the same postinoculation time.

With our preparations, we encountered a total of 17 HEV-infected pyramidal cells and eight longitudinally cut axons belonging to the infected pyramidal cells. More than 200 photographs, both lower and higher magnifications, have been taken of each cell, and all the axons and cells have been thoroughly examined and analyzed.

Transport of HEV in the axons

HEV particles were observed in the axon hillocks, the initial segments (Fig. 1F), and the distal myelinated axons (Fig. 1G,H). The number of virus particles varied from axon to axon, but all the virus particles in the axoplasm were enclosed within smooth-surfaced vesicles, some of

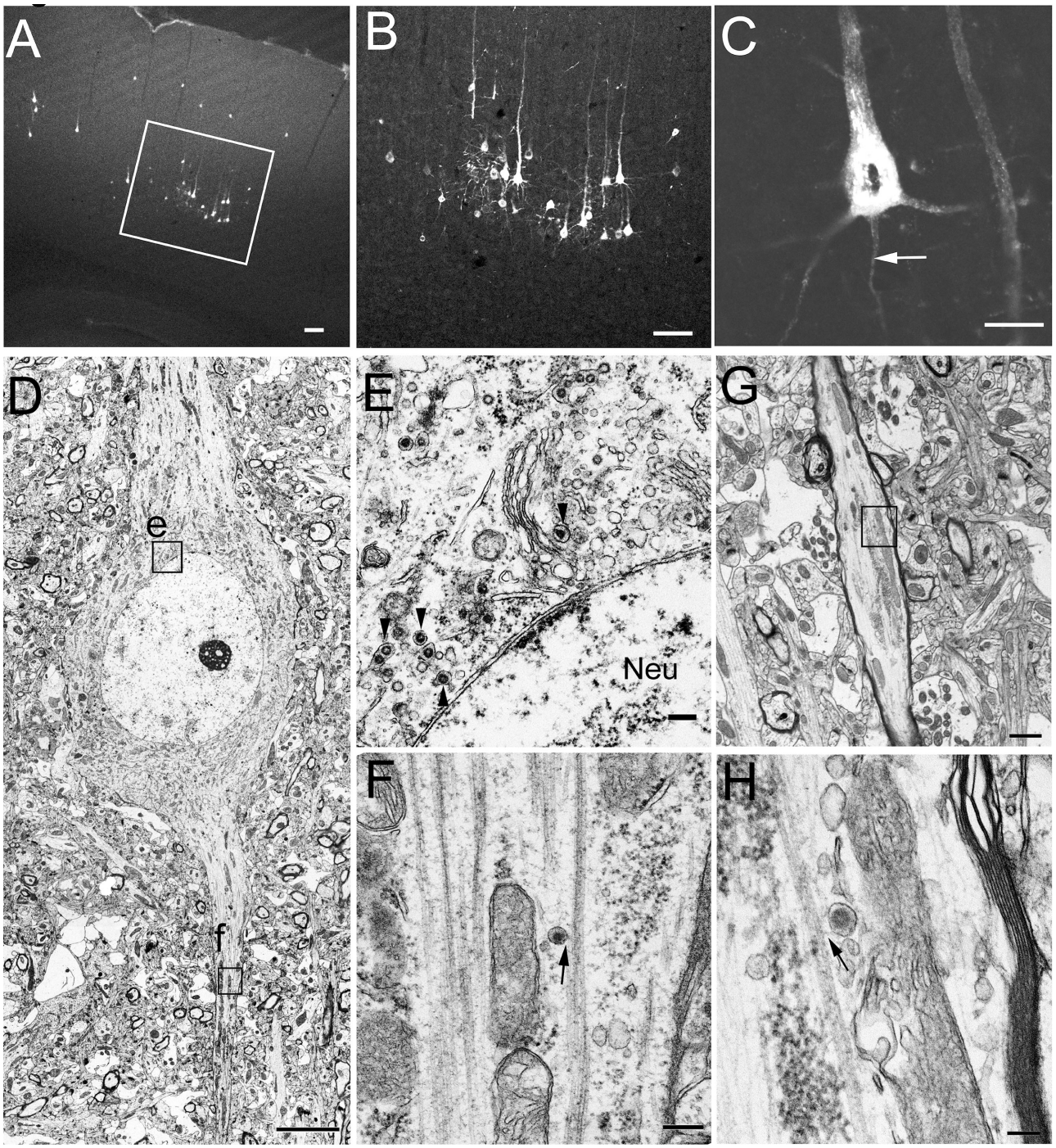

Figure 1. HEV-infected neurons in the primary motor cortex at day 4 p.i. **A–C**: Fluorescence micrographs showing HEV-infected neurons in the primary motor cortex at day 4 p.i. A is a low-magnification micrograph, and the boxed area is enlarged in B, showing that infected neurons are located mainly in layer V of the primary motor cortex. C is an image of a 0.6-μm-thick optical section, showing the punctuate cytoplasmic staining of HEV, which is distributed throughout the cell body, dendrites, and axon (arrow). **D–H**: EM photomicrographs showing HEV particles in infected pyramidal cells. D shows an infected pyramidal cell, in which both progeny virions and budding profiles are observed in the somatodendritic cytoplasm. The boxed area e is enlarged in E, showing virus particles present in small vesicles (arrowheads) in the perikaryon of the pyramidal cell. No virus particles are found in the nuclei (Neu). The boxed area f is enlarged in F, showing an HEV particle within a small vesicle (arrow), which is closely associated with the fasciculated microtubules in the initial segment. G shows a longitudinally cut myelinated axon of an infected pyramidal cell. The boxed area is enlarged in H, showing a virus-containing vesicle (arrow) closely associated with the microtubules. Scale bars = 100 μm in A,B; 20 μm in C; 5 μm in D; 200 nm in E,F; 1 μm in G; 100 nm in H.

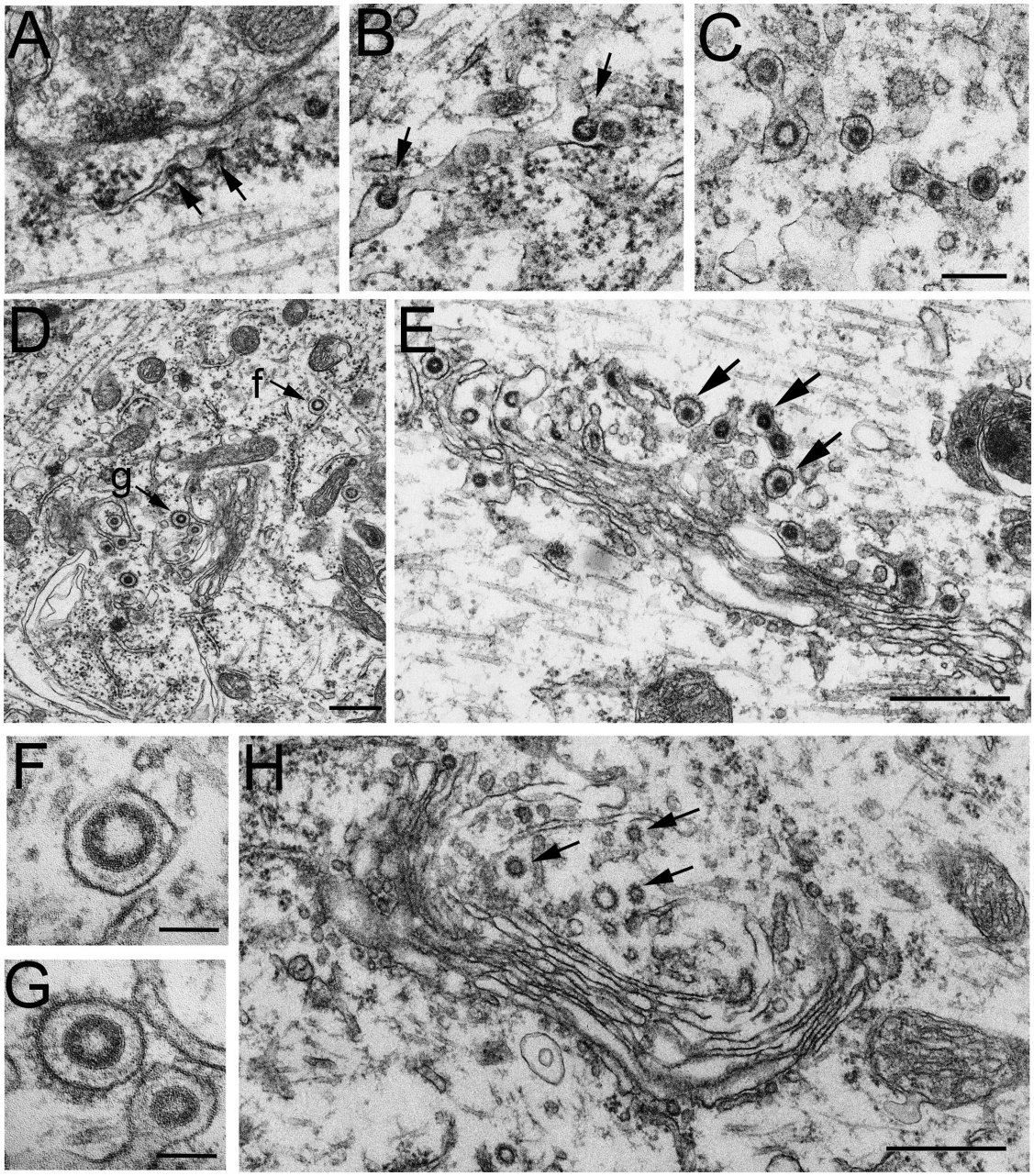

Figure 2. EM photomicrographs showing the replication and assembly of HEV in pyramidal cells. Viral assembly inside the infected cells is initiated by an electron-dense crescent segment (arrows in A), which is attached to the external membrane of the ER cistern. Larger crescent segments (arrows in **A,B**) bulge into the lumen of the ER cistern by incorporation of the lipid bilayer of the ER into the viral envelope. Short stalks (arrows in B) are found still continuing with the ER membrane. The virus particles in the lumen of the ER cistern are covered with well-defined surface projections (**C**). **D** shows virus particles in Golgi and ER areas in the perikaryal cytoplasm of a pyramidal cell. No membranous decorations are present on the outer surface of the virus-containing vesicle near the ER cistern (indicated by f, and enlarged in F). By contrast, the virion in the Golgi area (indicated by g, and enlarged in G) is enclosed within a vesicle with spinule coats on the outer surface. In both cases, a layer of surface projections is seen surrounding the viral envelope beneath the vesicle membrane (**F,G**). **E** shows a Golgi apparatus in the primary dendrite of a proximal cell, where viral budding profiles are observed in the lateral rims of the Golgi cisternae, and virus particles are present in the dilated cisternae of the Golgi network. On the trans-side of the Golgi complex, enveloped virions are enclosed within small vesicles (arrows), with small spinule coats on the outer surface. **H** shows a Golgi apparatus in the perikaryal cytoplasm of a pyramidal cell from the vehicle control. The trans-Golgi network and some small vesicles nearby possess small spinule coats on their cytoplasmic surface (arrows) but contain no virus-like particles. Scale bars = 200 nm in A–C; 500 nm in D,E,H; 100 nm in F,G.

which were found closely associated with microtubules (arrows in Fig. 1F,H). Such microtubule-associated vesicles have been observed in all the axons examined, suggesting that the virus was being transported within the vesicles along the microtubules in the axons.

HEV assembly in the pyramidal cells

In pyramidal cells, HEV replication occurred mainly in the perikaryon and dendrites. The earliest sign of viral assembly observed inside infected cells was an electron-dense crescent segment indenting into the external

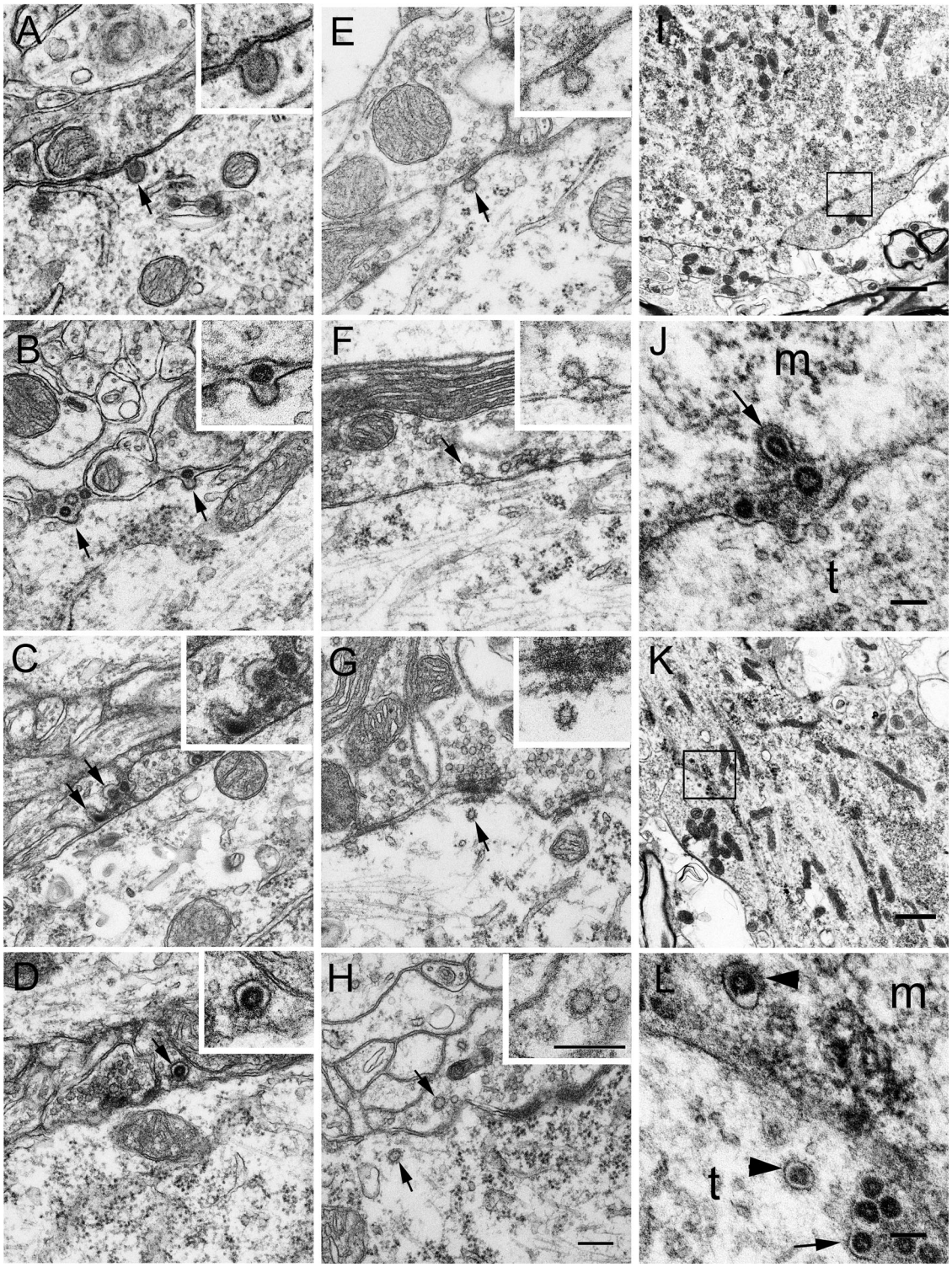

Figure 3.

membrane of ER cisternae in the perikaryal cytoplasm (Fig. 2A). Large crescent segments were observed bulging into the lumen of ERs by incorporating the lipid bilayer of the ER (Fig. 2B). As virus particles were internalized into the lumen of ERs, the lipid bilayer of ERs seemed to be gradually pinched off and finally fused around the virus particles (Fig. 2C,D).

With the progression of infection, large numbers of virions were packed individually in vesicles in the trans-Golgi networks (Fig. 2E). Some of the vesicles were decorated with small spinule coats around their outer surfaces (arrows in Fig. 2E), which were about 10–15 nm long and exhibited the morphology characteristic of clathrin (Fig. 2G). Such coated vesicles were observed throughout the cytoplasm of the perikarya and dendrites and appeared abundant near the Golgi complexes (Fig. 2D,E).

The diameters of virions and virion-containing vesicles in two representative infected pyramidal cells were measured under ×30,000 magnification on electron micrographs. HEV virions ranged from 60 to 120 nm in diameter (72.8 ± 11.2 nm, mean ± SD, n = 60), whereas the virion-containing vesicles ranged from 90 to 180 nm in diameter (125.1 ± 19.7 nm, mean ± SD, n = 94).

HEV dissemination in the motor cortex

Morphological analysis suggested that coated vesicles played a pivotal role in both the egress and the subsequent entry of HEV. The coated vesicles, with one virion within one vesicle, were distributed beneath the cell surface of infected cells, and some of them were found apparently fusing with the plasma membrane (Fig. 3A). Through the openings at the fusion sites, progeny virions seemed to be released outside, whereas the membranous coating still remained at the release sites (Fig. 3B). No virus particles were observed in the adjacent axonal terminals, so the extracellular virus particles were thought to be the progeny virions that had been liberated from the infected pyramidal cells. In the synaptic clefts, virus particles were found trapped in the invaginations of the presynaptic membrane, where new membranous coating was seen on the cytoplasmic side (Fig. 3C).

Coated vesicles enclosing a single virion were further found in the axonal terminals adjacent to infected pyramidal cells (Fig. 3D). Extracellular virions were not enclosed by any vesicular structures, whereas vesicle-enclosed virus particles were otherwise observed in the axonal terminals touching on the infected neurons, so it seemed that the virions within the synapses had acquired new vesicular membrane after entry.

Possibly because of the accumulation of extracellular virions, the synaptic clefts became aberrantly dilated and had lost their normal integrities. On the other hand, infected astrocytes were not seen, even in the late stage of infection (data not shown). Transsynaptic transfers of HEV were demonstrated undoubtedly in nine pyramidal cells. Although only nine pyramidal cells were counted, the other cells were not included in the analysis not because HEV showed different transfer means in them but because the pre- or postsynaptic invaginations were not very clear because of the sectioning directions or because the virus particles were not located exactly nearby the pre- or postsynaptic invaginations.

Figure 3. HEV dissemination in the CNS. **A–D**: EM photographs from infected pyramidal cells showing the egress and entry of progeny virions. A shows an infected pyramidal cell, in which virus particles are observed within vesicles in the perikaryal cytoplasm. Near the cell surface, a virus-containing coated vesicle is found attaching to the plasma membrane (arrow; see also the **inset** for details). This coated vesicle is apparently fusing with the plasma membrane, and there is an opening at the fusion site. Notably, no virus is found in the adjacent neuropils. B shows the primary dendrite of an infected pyramidal cell. Several progeny virions are found extracellularly near the fusion sites, where a layer of coats still remain on the plasma membrane (arrows). The virion labeled by right arrow is enlarged in the **inset**. No virus is found either in the adjacent axonal terminals or in the surrounding glial processes. C shows extracellular virions in the dilated synaptic clefts, and some of them are trapped in the coated invaginations of the presynaptic membrane (arrows; see also the **inset** for details). D shows a virion within a coated vesicle (arrow; see also the **inset** for details) in the axon terminal adjacent to an infected pyramidal cell. **E–H**: Electron photographs from vehicle controls showing coated structures in the pre- and postsynaptic cytoplasm. E shows a coated invagination (arrow) in the postsynaptic membrane of a pyramidal cell. The bulbous portion of the invagination communicates with the extracellular synaptic cleft via a thin neck (see the **inset** for details). F shows a coated invagination (arrow) in the presynaptic membrane, which is further enlarged in the **inset**. G shows a coated vesicle (arrow) in the postsynaptic cytoplasm, which is further enlarged in the **inset**. H shows coated vesicles (arrows) present in both the pre- and the postsynaptic cytoplasm. The coated vesicle in the presynaptic region is further enlarged in the **inset**. **I–L**: HEV in spinal motoneurons. Three infected rats were perfused at day 3 p.i. with 4% paraformaldehyde in 0.1 M PB. Spinal segments at the level of ~L5–L6 were dissected and examined by EM. I and K show two α-motoneurons in the ventral horn of spinal cord. The boxed areas in I and K are enlarged in J and L, respectively. J shows a virus-containing coated vesicle (arrow) in the motoneurons attaching to the membrane. Virus particles without any vesicular structures are found extracellularly in the synaptic cleft. m, Neuronal cell body; t, axonal terminal. In L, coated vesicles (arrowheads) containing virus particles are seen both in the neuronal cytoplasm (m) and in an adjacent axonal terminal (t). In addition, many virions are accumulated in the dilated synaptic clefts, and some of them are seen trapped in the coated invaginations (arrows) of the axonal membrane. Scale bars = 200 nm in H (applies to A–H); 400 nm in inset H (applies to insets A–H); 1 μm in I,K; 100 nm in J,L.

Coated vesicular structures in the CNS

In uninfected pyramidal cells from the controls, the trans-Golgi network and some small vesicles in Golgi regions often possessed membranous decorations on parts of their surface, but no peri-Golgi vesicles containing viruses were observed (Fig. 2H). Coated vesicles were frequently encountered in either the pre- or the postsynaptic cytoplasm (Fig. 3G,H). Coated invaginations were also found in pre- and postsynaptic membranes (Fig. 3E,F). They were continuous with the synaptic cleft by a thin neck. However, no virus particles were found within either the coated vesicles or the invaginations.

Examples of coated vesicles and invaginations were found in the pre- or postsynaptic regions in all the samples from the controls. The diameters of coated vesicles, from three representative pyramidal cells, were measured under $\times$30,000 magnification on electron micrographs. They were 51.2 $\pm$ 18.7 nm (mean $\pm$ SD, n = 60) in diameter, significantly smaller than the virus-containing vesicles ($P < 0.5$, *t*-test).

To make clear whether the findings in the motor cortex could be generalized to other parts of the CNS, the spinal cords from three paraformaldehyde-fixed rats used for another experiment were also examined by EM. α-Motoneurons located in the ipsilateral ventral horn were constantly infected at day 3 p.i. Both the replication and the dissemination of HEV in the motoneurons were similar to those found in the pyramidal cells (Fig. 3I–L).

DISCUSSION

The present study examines the assembly and dissemination of coronavirus HEV 67N in the rat CNS, specifically the motor cortex. HEV virions initially budded from endoplasmic reticulum–Golgi intermediate compartments in the neurons and were assembled within coated vesicles through Golgi complexes. Progeny HEV virions were exocytosed from the host neuronal cells, possibly by use of the coated vesicles, and entered into the next-order neurons by endocytosis, again with the help of the coated vesicles (Fig. 4).

To the best of our knowledge, this means of dissemination used by HEV in the CNS is largely different from the means reported for the well-known neurotropic viruses herpesviruses and rhabdoviruses. Herpesviruses, including herpes simplex virus-1 and pseudorabies virus, also exploit exocytosis for egress from the host neuronal cells, but their subsequent entry into the synapse-linked neurons occurs exclusively by fusion of the virus envelope with the axonal membrane (Card et al., 1993; Diefenbach et al., 2008). Because of the direct penetration by fusion of herpesviruses, only virus nucleocapsids can gain access to the axoplasm (Dolivo et al., 1978; Marchand and Schwab, 1986; Card et al., 1993). On the other hand, rhabdoviruses, such as vesicular stomatitis virus and rabiesvirus, are released from the host neuronal cells by directly budding from the membrane of the neurons and subsequently endocytosed within vesicles by adjacent axonal terminals (Iwasaki and Clark, 1975; Dal Canto et al., 1976; Charlton and Casey, 1979; Superti et al., 1987; Lewis and Lents, 1998; Sun et al., 2005).

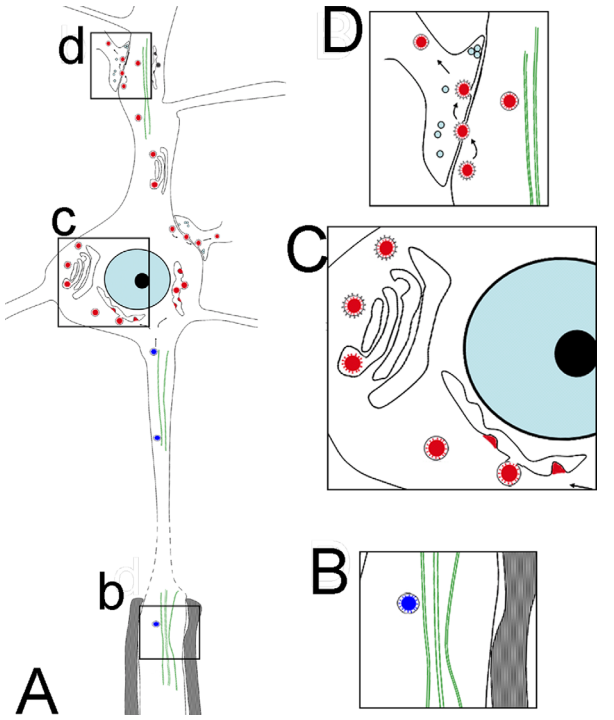

Figure 4. Hypothetical schematic showing the transport, replication, and transfer of HEV in the CNS. HEV is retrogradely transported inside vesicular structures by microtubules along the axon into the neuronal cell body (boxed area b in **A**, enlarged in **B**). Virions are replicated in the endoplasmic reticulum–Golgi intermediate compartments, packed into coated vesicles mainly through the Golgi complexes (boxed area c in A, enlarged in **C**). The progeny virions were released from the host cells by fusion of the coated vesicles with the plasma membrane and subsequently taken up by the next-order neurons by way of the membranous-coating-mediated endocytosis (boxed area d in A, enlarged in **D**). [Color figure can be viewed in the online issue, which is available at wileyonlinelibrary.com.]

The general features of HEV development observed in this study are largely consistent with those reported in previous investigations of coronavirus morphogenesis (Hobman, 1993; de Haan and Rottier, 2005; Masters, 2006). These previous studies have demonstrated that coronavirus morphogenesis takes place predominantly at smooth-walled, tubulovesicular membranes located intermediately between the rough ER and the Golgi complex. Immature virions in pre-Golgi compartments and Golgi cisternae are further subject to a postbudding maturation process in the trans-Golgi network and are finally

assembled in vesicles with or without clathrin coating (Chasey and Alexander, 1976; Tooze et al., 1987; Salanueva et al., 1999).

Studies on mouse hepatitis virus and transmissible gastroenteritis virus in vitro showed that progeny virions, collected in groups within one large vesicle lacking clathrin coats, were transported along the constitutive exocytic route to the host cell surface and were liberated by the fusion of the vesicle membrane with the plasma membrane (Tooze et al., 1987; Salanueva et al., 1999). Our recent study on HEV in rat DRG showed that this is also true for HEV in the sensory neurons, where the progeny virions were released in groups by the large-vesicle-mediated fusion (Li et al., 2012).

On the other hand, some coronaviruses, such as infectious avian bronchitis virus (Beaudette strain), have been reported to be able to leave the host cells by coated vesicle-mediated exocytosis (Chasey and Alexander, 1976). This is the case for HEV in the pyramidal cells, insofar as the present study showed that both the entry and the egress of HEV were mediated by coated vesicles, which differs from the large vesicles reported previously in that they are much smaller, bear a fuzzy coat, and usually contain only one virion. Given that coronaviruses depend on assistance from the host cell in virtually all stages of the infection, it seems conceivable that the means used even by the same virus for dissemination may differ within different cell types (Hobman, 1993; Masters, 2006).

The cell bodies of DRG neurons relay sensory information from the periphery to the CNS and are surrounded by a unique glial envelope formed by satellite cells (Hanani, 2005). Because no synaptic structures are present in the DRGs, the released HEV virions from the sensory neurons were subsequently phagocytosed by the adjacent satellite cells, which are now known not merely to give mechanical or nutrient support to the neurons but also to have a scavenging function to control the extracellular microenviroment around the neurons (Hanani, 2005; Li et al., 2012).

In comparison, the neurons in the CNS are linked functionally together by synaptic junctions, where nerve impulses are transmitted from one nerve cell to another. Increasing data suggest that synapses may also function as a preferential site of interneuronal exchange (Charlton and Gray, 1966; Waxman and Pappas, 1969; Grafstein, 1971; Waxman et al., 1980; Davis and McKinnon 1982; Trojanowski and Schmidt, 1984; Luo and Dessem, 1996; Spacek and Harris 2004). Many EM investigations have demonstrated the presence of coated vesicular invaginations as a general feature of both the pre- and postsynaptic membranes (Charlton and Gray, 1966; Waxman and Pappas, 1969; Waxman et al., 1980; Spacek and Harris 2004). Moreover, studies utilizing a variety of tracing molecules have shown significant transsynaptic labeling after intracellular injection, indicating that interneuronal transfer indeed occurs at the synaptic junctions (Grafstein, 1971; Davis and McKinnon 1982; Trojanowski and Schmidt, 1984; Luo and Dessem, 1996). However, the transsynaptic process is complicated and not easy to study, partially because of the small but complex structure of the synapse and the lacking of effective tracing methods.

Coronaviruses, which are about 100 nm in diameter, have the largest RNA genomes (27–32 kb) known to date and can be recognized by EM without labeling (Masters, 2006). Moreover, their life cycle has been shown to rely virtually completely on the cellular events preexisting in the host cells (Hobman, 1993; Pelkmans and Helenius, 2003; Masters, 2006). Therefore, coronaviruses are re-emerging as a useful molecular and cellular tool for analyzing a variety of complex cellular processes (Tooze et al., 1987; Pelkmans and Helenius, 2003).

Overall, the present study on HEV has provided additional evidence that membranous-coating-mediated endo-/exocytosis can be used for the transsynaptic exchanges of coronaviruses. In addition, our results suggested that the transsynaptic pathway has the capability of being adapted for larger granular materials, such as viruses. Our study contributes high-resolution morphological data relevant for understanding the mechanisms underlying coronavirus infections as well as the intercellular exchanges occurring at the synaptic junctions.

LITERATURE CITED

Andries K, Pensaert MB. 1980. Immunofluorescence studies on the pathogenesis of hemagglutinating encephalomyelitis virus infection in pigs after oronasal inoculation. Am J Vet Res 41:1372–1378.

Bai WZ, Hirano N, Taniguchi T, Tohyama K, Hashikawa T. 2006. Spatial and time-dependent transneuronal propagation of swine coronavirus (hemagglutinating encephalomyelitis virus, HEV) in the rat central nervous system after its hind footpad inoculation. Neurosci Res 55:S106–S106.

Card JP, Rinaman L, Lynn RB, Lee BH, Meade RP, Miselis RR, Enquist LW. 1993. Pseudorabies virus infection of the rat central nervous system: ultrastructural characterization of viral replication, transport, and pathogenesis. J Neurosci 13:2515–2539.

Charlton KM, Casey GA. 1979. Experimental rabies in skunks: immunofluorescence light and electron microscopic studies. Lab Invest 41:36–44.

Charlton BT, Gray EG. 1966. Comparative electron microscopy of synapses in the vertebrate spinal cord. J Cell Sci 1:67–80.

Chasey D, Alexander DJ. 1976. Morphogenesis of avian infectious bronchitis virus in primary chick kidney cells. Arch Virol 52:101–111.

Clarke JK, McFerran JB. 1971. An electron microscopic study of haemagglutinating encephalomyelitis virus of pigs. J Gen Virol 13:339–344.

Dal Canto MC, Rabinowitz SG, Johnson TC. 1976. In vivo assembly and maturation of vesicular stomatitis virus. Lab Invest 35:515–524.

Davis JN, McKinnon PN. 1982. Anterograde and transcellular transport of a fluorescent dye, bisbenzimide, in the rat visual system. Neurosci Lett 29:207–212.

de Groot RJ, Baker SC, Baric R, Enjuanes L, Gorbalenya A, Holmes KV, Perlman S, Poon L, Rottier PJM, Talbot PJ, Woo PCY, Ziebuhr J. 2012. Coronaviridae. In: King AMQ, Adams M J, Carstens EB, Lefkowitz EJ (eds). Virus taxonomy, classification and nomenclature of viruses, ninth report of the International Committee on Taxonomy of Viruses, International Union of Microbiological Societies, Virology Division. Waltham, MA: Elsevier Academic Press. p 806–828.

de Haan CA, Rottier PJ. 2005. Molecular interactions in the assembly of coronaviruses. Adv Virus Res 64:165–230.

Diefenbach RJ, Miranda-Saksena M, Douglas MW, Cunningham AL. 2008. Transport and egress of herpes simplex virus in neurons. Rev Med Virol 18:35–51.

Dolivo M, Beretta E, Bonifas V, Foroglou C. 1978. Ultrastructure and function in sympathetic ganglia isolated from rats infected with pseudorabies virus. Brain Res 140: 111–123.

Grafstein B. 1971. Transneuronal transfer of radioactivity in the central nervous system. Science 172:177–179.

Greig AS, Mitchell D, Corner AH, Bannister GL, Meads EB, Julian RJ. 1962. A hemagglutinating virus producing encephalomyelitis in baby pigs. Can J Comp Med Vet Sci 26: 49–56.

Hanani M 2005. Satellite glial cells in sensory ganglia: from form to function. Brain Res Brain Res Rev 48:457–476.

Hobman TC 1993. Targeting of viral glycoproteins to the Golgi complex. Trends Microbiol 1:124–130.

Hirai K, Chang CN, Shimakura S. 1974. A serological survey on hemagglutinating encephalomyelitis virus infection in pigs in Japan. Nippon Juigaku Zasshi 36:375–380.

Hirano N, Ono K, Takasawa H, Murakami T, Haga S. 1990. Replication and plaque formation of swine hemagglutinating encephalomyelitis virus (67N) in swine cell line, SK-K culture. J Virol Methods 27:91–100.

Hirano N, Haga S, Fujiwara K. 1994. The route of transmission of hemagglutinating encephalomyelitis virus (HEV) 67N strain in 4-week-old rats. Adv Exp Med Biol 342:333–338.

Hirano N, Nomura R, Tawara T, Ono K, Iwasaki Y. 1995. Neuronal spread of swine hemagglutinating encephalomyelitis virus (HEV) 67N strain in 4-week-old rats. Adv Exp Med Biol 380:117–119.

Iwasaki Y, Clark HF. 1975. Cell to cell transmission of virus in the central nervous system. II. Experimental rabies in mouse. Lab Invest 33:391–399.

Lewis P, Lentz TL. 1998. Rabies virus entry into cultured rat hippocampal neurons. J Neurocytol 27:559–573.

Li YC, Bai WZ, Hirano N, Hayashida T, Hashikawa T. 2012. Coronavirus infection of rat dorsal root ganglia: ultrastructural characterization of viral replication, transfer, and the early response of satellite cells. Virus Res 163:628–635.

Luo P, Dessem D. 1996. Transneuronal transport of intracellularly injected biotinamide in primary afferent axons. Brain Res Bull 39:323–334.

Marchand CF, Schwab ME 1986. Binding, uptake and retrograde axonal transport of herpes virus suis in sympathetic neurons. Brain Res 383:262–270.

Masters PS. 2006. The molecular biology of coronaviruses. Adv Virus Res 66:193–292.

Mengeling WL, Boothe AD, Ritchie AE. 1972. Characteristics of a coronavirus (strain 67N) of pigs. Am J Vet Res 33:297–308.

Meyvisch C, Hoorens J. 1978. An electron microscopic study of experimentally induced HEV encephalitis. Vet Pathol 15: 102–113.

Pelkmans L, Helenius A. 2003. Insider information: what viruses tell us about endocytosis. Curr Opin Cell Biol 15: 414–422.

Salanueva IJ, Carrascosa JL, Risco C. 1999. Structural maturation of the transmissible gastroenteritis coronavirus. J Virol 73:7952–7964.

Spacek J, Harris KM. 2004. Trans-endocytosis via spinules in adult rat hippocampus. J Neurosci 24:4233–4241.

Sun X, Yau VK, Briggs BJ, Whittaker GR. 2005. Role of clathrin-mediated endocytosis during vesicular stomatitis virus entry into host cells. Virology 338:53–60.

Superti F, Seganti L, Ruggeri FM, Tinari A, Donelli G, Orsi N. 1987. Entry pathway of vesicular stomatitis virus into different host cells. J Gen Virol 68:387–399.

Tooze J, Tooze SA, Fuller SD. 1987. Sorting of progeny coronavirus from condensed secretory proteins at the exit from the trans-Golgi network of AtT20 cells. J Cell Biol 105: 1215–1226.

Trojanowski JQ, Schmidt ML. 1984. Interneuronal transfer of axonally transported proteins: studies with HRP and HRP conjugates of wheat germ agglutinin, cholera toxin and the B subunit of cholera toxin. Brain Res 311:366–369.

Waxman SG, Pappas GD. 1969. Pinocytosis at postsynaptic membranes: electron microscopic evidence. Brain Res 14: 240–244.

Waxman SG, Waxman M, Pappas GD. 1980. Coordinated micropinocytotic activity of adjacent neuronal membranes in mammalian central nervous system. Neurosci Lett 20: 141–146.

Yagami K, Hirai K, Hirano N. 1986. Pathogenesis of haemagglutinating encephalomyelitis virus (HEV) in mice experimentally infected by different routes. J Comp Pathol 96: 645–657.

Yagami K, Izumi Y, Kajiwara N, Sugiyama F, Sugiyama Y. 1993. Neurotropism of mouse-adapted haemagglutinating encephalomyelitis virus. J Comp Pathol 109:21–27.